A&A 407, 713–723 (2003)
DOI: 10.1051/0004-6361:20030914

Astronomy & Astrophysics

A simple analytical expression for the power spectrum of cascading Alfvén waves in the solar wind

R. Vainio[1], T. Laitinen[2], and H. Fichtner[3]

[1] Theoretical Physics Division, Department of Physical Sciences, University of Helsinki, Finland
[2] Space Research Laboratory⋆, Department of Physics, University of Turku, Finland
[3] Institut für theoretische Physik IV: Weltraum- und Astrophysik, Ruhr-Universität Bochum, 44780 Bochum, Germany

Received 3 March 2003 / Accepted 4 June 2003

Abstract. Alfvén wave transport in the solar wind, including non-linear spectral energy transfer, is studied. We present numerical solutions of wave transport using a diffusive flux function previously introduced for spectral energy transfer, and compare it with the analytical solution obtained for a convective flux function. The two models of cascading produce very similar behavior of a power spectrum initially of $1/f$-form at the solar surface, provided that the cascading constants are tuned to produce the same spectral flux in the inertial range. We present an analytical expression for the power spectrum of the diffusively-cascading Alfvén waves in the solar wind derived from a solution of the wave transport equation and show that it compares well with the exact solutions. Our expression enables (semi) analytical evaluation of the cyclotron heating rate, the wave pressure gradient, and the energetic-particle mean free path related to the Alfvén waves in the corona and solar wind.

Key words. Sun: corona – Sun: particle emission – Sun: solar wind – turbulence

1. Introduction

One of the fundamental outstanding problems in solar physics, even about half a century after its formulation, is a clearcut identification of the mechanism(s) that heat the solar corona to such high temperature that it expands as a solar wind into the surrounding interstellar medium. In the context of studies of the solar wind many suggestions have been made such as MHD or acoustical wave energy (van de Hulst 1953), electron heat conduction (Chapman 1957), plasma wave damping (Hartle & Barnes 1970), resonant ion-cyclotron interactions (Hollweg & Turner 1978) or velocity filtration (Scudder 1992). Out of the many proposed candidates few have survived and among those the most promising one is the damping of ion-cyclotron waves as is discussed, along with an extended review of related work, by Hollweg & Isenberg (2002).

Laitinen et al. (2003) have recently discussed various approaches employed for an explicit incorporation of the process of ion-cyclotron damping into kinetic (e.g. Isenberg 2001), semi-kinetic (e.g. Vocks & Marsch 2001) or hybrid (e.g. Liewer et al. 2001), and fluid models (e.g. Hu et al. 1999) of solar wind expansion. Aiming at a study of the mutual implications of models of the solar wind heating and of the coronal and interplanetary transport of energetic particles, their focus was on fluid models. So far, only fluid models allow one to investigate the effects of processes acting close to the coronal base on the plasma at heliocentric distances r of 0.3 AU and beyond. Therefore, they play a privileged role when trying to relate in-situ measurements at $r > 0.3$ AU to remote observations of the acceleration region of the solar wind at $r < 10\ r_\odot$, with $r_\odot$ denoting the solar radius.

The incorporation of ion-cyclotron damping into fluid models requires the definition of specific acceleration as well as heating functions describing the deposition of wave momentum and energy into the solar wind plasma. Laitinen et al. (2003) classified the various corresponding modeling attempts by distinguishing between ad-hoc, phenomenological, and consistent heating functions. The ad-hoc heating functions, originally introduced by Hartle & Barnes (1970), are formulated without explicitly specifying a physical process and do not depend on the plasma parameters. While the phenomenological heating functions introduced by Hollweg (1986) explicitly relate the plasma heating to the turbulent transport of waves through the solar wind, this process is formulated by prescribing a correlation length scale for the waves. Consistent heating functions require a description of this parameter in terms of the wave energy and solar wind parameters. For an appropriate description of the wave power within a fluid concept, Tu et al. (1984) derived an equation that contains its spatial transport in the magnetized expanding solar wind plasma as well as its transport in

Send offprint requests to: R. Vainio,
e-mail: rami.vainio@helsinki.fi

⋆ SRL is part of the Väisälä Institute for Space Physics & Astronomy, University of Turku, Finland.

wave number space, thus providing an explicit formulation of the physics of the cascade.

In the context of the heating of the solar wind plasma, not only was the importance of the wave power transport in wave number space recognized early, but also an equation describing the phase space evolution of the wave power was derived almost 20 years ago (Tu et al. 1984). Its first consistent solution was presented by Tu (1987) for a one-fluid model. The consistent solution for a two-fluid description, however, was not obtained until recently (Hu et al. 1999). These authors solved the wave power evolution equation simultaneously with the wind equations for the whole region from the coronal base to the Earth's orbit. The description of the transport in wave number space, usually referred to as cascading, was based on so-called cascade functions derived by Tu et al. (1984) and Tu (1987, 1988). Zhou & Matthaeus (1990) pointed out that these cascade functions belong to a specific class of models describing MHD turbulence, and that there exists an alternative, if not more general, approach. This approach is based on a diffusion approximation for the spectral transfer of wave energy first introduced by Leith (1967) who was motivated by the successful application of this idea in radiation as well as neutron transport theory in the 1950s. This *diffusive cascading* is superior to the previously used approach, which we refer to as *convective cascading*, in that it yields vanishing transport in wave number for flat power spectra, i.e., it preserves the equilibrium in the case of no damping.

While the diffusive cascading, as proposed by Zhou & Matthaeus (1990) for the case of interplanetary MHD turbulence, has been employed for the acceleration of solar flare particles (Miller & Roberts 1995), it has not yet been consistently incorporated into models of solar wind expansion. Before adding the diffusive cascading term to the wave power evolution equation and numerically solving the latter simultaneously with the wind equations, as done for the convective cascading by Hu et al. (1999), however, a study of the principal consequences of diffusive cascading for the heating of the solar wind, for the wave pressure (gradient) and for the mean free path of energetic particles is helpful. This is not only because of the usefulness of the insights one obtains from a test wave approach (in which the fluid properties are prescribed, i.e., not consistently computed), but also because it results in a valuable analytical approximation of the evolution of the power spectrum of Alfvén waves in the solar wind.

Therefore, after a description of a simplified solar wind model and a brief review of the convective and diffusive cascading approaches in Sect. 2, we present in Sect. 3 an analytical expression for the wave power spectrum in the case of diffusive cascading, very similar to the known analytical steady state (test-wave) solution of the convective cascade, which we re-derive for the Kolmogorov phenomenology. In Sect. 4, based on this approximation, we demonstrate both the near-equivalence of diffusive and convective cascading and the goodness of the analytical approximation derived in Sect. 3. We then apply the approximation to the computation of the resulting heating functions, the wave pressure gradient, as well as the mean free path of energetic particles. All findings are discussed along with the conclusions in Sect. 5.

2. Models

2.1. Coronal and solar wind plasma

While it is possible to numerically solve the multi-fluid equations describing a plasma heated by cascading cyclotron waves in a given magnetic-field geometry (e.g., Hu et al. 1999), such an effort is beyond the scope of the present analysis. Instead, we use prescribed models of the solar corona and solar wind. For slow solar wind, we have devised a model that is computationally simple but, nonetheless, represents quite well the observations of the equatorial regions. Note, however, that we employ this simplified solar wind model below only for the numerical cascade simulations. The analysis is conducted for general solar wind parameters.

We start our modeling from three simplifying assumptions: we take (i) the plasma to be an electron-proton plasma, (ii) the central magnetic field line of a considered flux tube to be radial, and (iii) the sum of solar wind and Alfvén speeds, $V \equiv u + v_\mathrm{A}$, i.e., the phase and group speed of the outward-propagating Alfvén waves, to be constant. In addition, we use the conservation of particle number, $An_\mathrm{e}u = \text{const.}$, to calculate the solar wind speed (assumed to be the same for both species), the Alfvén speed, and the electron number density, n_e, as functions of radial distance r from the center of the Sun. Here, $A(r) \propto 1/B$ is the cross-sectional area of the flux tube, and $B(r)$ is the magnetic field on the considered line of force, modeled by

$$B(r) = B_0 \frac{r_0^2}{r^2}\left[1 + 1.9\, b_\mathrm{f}\left(\frac{r_\odot}{r}\right)^6\right], \tag{1}$$

where b_f is a parameter describing the magnetic field close to the coronal base. All quantities with subscripts 0 denote values at 1 AU. We obtain

$$v_\mathrm{A} = v_\mathrm{A0}\frac{v_\mathrm{A0}B}{2u_0B_0}\left[\sqrt{1+\left(\frac{u_0}{v_\mathrm{A0}}+1\right)\frac{4u_0B_0}{v_\mathrm{A0}B}}-1\right] \tag{2}$$

$$u = V - v_\mathrm{A} \tag{3}$$

$$n_\mathrm{e} = n_\mathrm{e0}\frac{Bu_0}{B_0u}. \tag{4}$$

Thus, fixing the parameters V, v_A0, n_e0 and b_f, and noting that $B_0 = v_\mathrm{A0}\sqrt{4\pi m_\mathrm{p} n_\mathrm{e0}}$ and $u_0 = V - v_\mathrm{A0}$, gives us a description of the coronal and solar wind plasma, which we employ in our numerical simulations of the cascading Alfvén waves.

The assumption (iii), regarding the constancy of the Alfvén-wave speed in the inertial frame, results in the model to be unable to fit the dilute fast solar wind streams, because they have too large Alfvén speeds in the corona. Thus, when discussing the applications of our model, fast winds are studied using the same magnetic field as above combined with the empirical polar-coronal hole density model of Sittler & Guhathakurta (1999). Using a given value for the solar wind speed at 1 AU together with the other assumptions (except (iii)) listed above then allows one to determine the solar wind speed profile.

An example of our models along with observational data is plotted in Fig. 1. The values chosen for the slow-wind model are $n_\mathrm{e0} = 10\ \mathrm{cm}^{-3}$, $V = 400\ \mathrm{km\ s}^{-1}$, $v_\mathrm{A0} = 20\ \mathrm{km\ s}^{-1}$, all consistent with measurements at 1 AU (Schwenn 1990), and

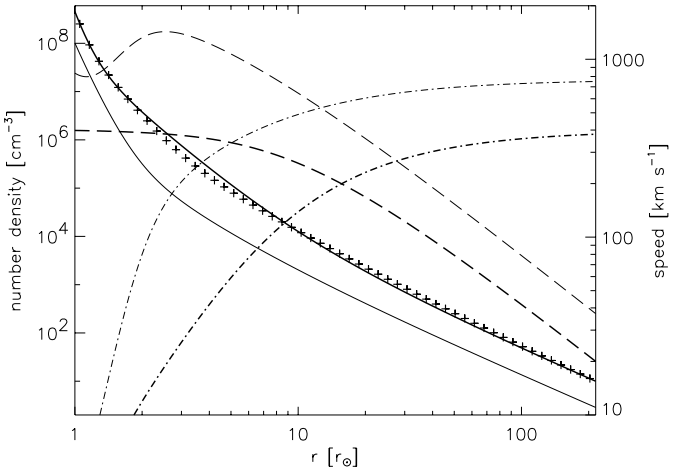

Fig. 1. Profiles of solar wind speed (dash-dotted curves), Alfvén speed (dashed curves), and number density (solid curves). The thick [thin] curves result from our slow [fast] solar wind model. A fit to the observational equatorial electron densities is denoted by crosses.

$b_f = 1$ reproducing the coronal base value of 4.54×10^8 cm^{-3} given by Bird & Edenhofer (1990) for the electron number density. The modeled slow-wind number density profile compares well with the observations at all distances. From the wealth of empirical density models summarized in Bird & Edenhofer (1990), we have chosen the Allen–Baumbach formula for the inner corona supplemented with a term proportional to $r^{-2.76}$ to reproduce, in the outer corona, the standard empirical model of Newkirk for the equatorial region during solar minimum and with a term proportional to r^{-2} to account for the asymptotic expansion at constant speed, which we have adjusted to yield the density of 10 cm^{-3} at 1 AU, consistent with the observations in low-speed streams (Schwenn 1990). The solar wind speed profile given by our slow-wind model gives a good eyeball fit to the widely scattered observational points given in Bird & Edenhofer (1990, Fig. 2.18). The implied magnetic field of 3.9 G at the coronal base is also in a reasonable range, at least for the quiet corona. The fast-wind profiles presented in Fig. 1 are given for $u_0 = 750$ km s^{-1}.

2.2. Alfvénic turbulence

As the model governing the power spectrum, $P(f, r)$, of Alfvénic turbulence we use that of Tu et al. (1984), which, in steady state, can be given by

$$\frac{v_A}{AV}\frac{\partial}{\partial r}\left(\frac{AV}{v_A}VP\right) = -\frac{\partial F}{\partial f}, \tag{5}$$

where f is the wave frequency in the inertial frame and F is the spectral flux function.

The difference between the convective and the diffusive treatment arises in the definition of the flux function. In the convective approach it is defined by Tu (1987, 1988) as

$$F = 2\pi C^2 \frac{v_A}{V}\frac{f^{5/2}P^{3/2}}{B}. \tag{6}$$

The resulting form of Eq. (5) then transports wave energy to higher frequencies until a steady-state spectrum $\propto f^{-5/3}$ is reached, thus reproducing the observations of MHD turbulence in the solar wind, which suggest the Kolmogorov phenomenology for the inertial-range spectrum (Horbury 1999).

The same steady state solution may also be reached with the diffusive approach, in which the flux function is defined by use of a diffusion coefficient as

$$F = -D_{ff}\frac{\partial P}{\partial f}, \quad \text{where} \tag{7}$$

$$D_{ff} = 2\pi\tilde{C}^2 \frac{v_A}{V}\frac{f^{7/2}P^{1/2}}{B}. \tag{8}$$

In this case, Eq. (5) represents diffusion in frequency space governed by the diffusion coefficient D_{ff}. The f-derivative of this flux function vanishes for two steady state solutions, $P \propto f^{-q}$: for a Kolmogorov spectrum, $q = 5/3$, and for a flat spectrum, $q = 0$.

The flux function in both formulations is proportional to a model parameter, $C^2(r) = \alpha\alpha_1(r)$ and $\tilde{C}^2(r) = \tilde{\alpha}\alpha_1(r)$, where α [$\tilde{\alpha}$] is the cascading constant in the convective [diffusive] approach and α_1 is the square root of the ratio of the intensities of the inward and outward propagating Alfvén waves (Verma et al. 1995). (Note that in previous work (e.g., Tu et al. 1984; Tu 1987; Hu et al. 1999), α_1 has often been taken to be directly proportional to the inward/outward ratio, but this is valid only in the case of the Kraichnan phenomenology (Verma et al. 1995).) As α_1 can not be calculated self-consistently in the present model we use instead the formulation by Hu et al. (1999):

$$\alpha_1(r) = \begin{cases} \alpha_0\left(\dfrac{r - r_\odot}{9r_\odot}\right)^\eta & r_\odot \le r < 10\,r_\odot \\ \alpha_0 & r \ge 10\,r_\odot. \end{cases} \tag{9}$$

Thus, because it *postulates* the intensity of the inward waves, this model can not address the important questions of how the ingoing waves are produced, how they propagate, or what their role is in the overall energy balance.

The value of $\alpha = 1.25$ – consistent with observations of ordinary fluid turbulence – in the convective flux function, Eq. (6), was derived from solar wind observations by Tu et al. (1989). We adopt this value for the convective cascade model. For the diffusive model, we choose $\tilde{\alpha} = \frac{3}{5}\alpha = 0.75$ to produce consistent values of the diffusive flux function given by Eqs. (7)–(8) in the inertial range, where $\partial P/\partial f \approx -(5/3)P/f$.

3. Analytical cascade formulation

3.1. Exact solution for the convective cascade

As was noted already by Tu et al. (1984), the convective cascade formulation in the test-wave approach is governed by a quasi-linear first-order partial differential equation that can be solved analytically using the method of characteristics. The solution was presented by Tu et al. (1984) for the Kraichnan cascade, where $F \propto f^3P^2$, and by Tu (1988) for the Kolmogorov cascade. We re-derive the solution here for the Kolmogorov cascade.

First note that the wave transport equation in the convective case can be written in a compact dimensionless form as

$$\frac{\partial I}{\partial \tau} - I^{1/2}\frac{\partial I}{\partial x} = 0. \tag{10}$$

Here, the dependent variable is

$$I(x,\tau) = \frac{V^2 B_\odot v_{\mathrm{A}\odot}}{V_\odot^2 B v_{\mathrm{A}}}\frac{f^{5/3}P(f,r)}{f_{\mathrm{n}}^{5/3}P(f_{\mathrm{n}},r_\odot)}, \tag{11}$$

where f_{n} is an arbitrarily chosen normalization frequency. The independent variables are

$$x = \left(\frac{f_{\mathrm{n}}}{f}\right)^{2/3} \tag{12}$$

and

$$\tau = 2\pi f_{\mathrm{n}}\epsilon_P^{1/2}\int_{r_\odot}^{r}\frac{C^2(r')V_\odot v_{\mathrm{A}}(r')}{V^3(r')}\left(\frac{n_{\mathrm{e}\odot}}{n_{\mathrm{e}}(r')}\right)^{1/4}\mathrm{d}r', \tag{13}$$

where $\epsilon_P \equiv f_{\mathrm{n}}P(f_{\mathrm{n}},r_\odot)/B_\odot^2 \ll 1$ is a dimensionless constant.

Equation (10) can be formally solved as

$$I(x,\tau) = g\left(x + I(x,\tau)^{1/2}\tau\right) \tag{14}$$

with the function

$$g(x) = I(x,0) = x^{-5/2}\frac{P\left(f_{\mathrm{n}}x^{-3/2},r_\odot\right)}{P(f_{\mathrm{n}},r_\odot)}. \tag{15}$$

This gives us an algebraic equation for $I(x,\tau)$, which may have to be solved numerically, depending on the form of $g(x)$.

Let us consider the case of

$$P(f,r_\odot) = \epsilon_P\frac{B_\odot^2}{f}. \tag{16}$$

(Note that an initial spectrum with this slope can not extend from $f = 0$ to ∞, but a cutoff at both high and low frequencies has to be assumed to avoid diverging wave pressure. This means that analytical modeling presented below will only be valid between these frequencies.) Then,

$$g(x) = 1/x \tag{17}$$

and

$$I(x,\tau)\left[x + I(x,\tau)^{1/2}\tau\right] = 1 \tag{18}$$

giving a cubic equation for $I(x,\tau)^{1/2}$. This can, of course, be solved exactly, but the asymptotic results are already evident from the equation itself.

At low frequencies, $x \gg I(x,\tau)^{1/2}\tau$, the solution is simply $I(x,\tau) \approx 1/x = I(x,0)$, which means that the waves propagate according to the WKB theory as

$$P(f,r) \approx P_{\mathrm{WKB}}(f,r) = P(f,r_\odot)\frac{B(r)\,V_\odot^2\,v_{\mathrm{A}}(r)}{B_\odot\,V^2(r)\,v_{\mathrm{A}\odot}}. \tag{19}$$

This approximation, thus, holds if $\tau \ll x^{3/2}$, i.e., if $f \ll f_{\mathrm{n}}/\tau(r) \equiv f_{\mathrm{c}}(r)$, which is given by

$$\frac{1}{f_{\mathrm{c}}} = 2\pi\epsilon_P^{1/2}\int_{r_\odot}^{r}\frac{C^2(r')V_\odot v_{\mathrm{A}}(r')}{V^3(r')}\left(\frac{n_{\mathrm{e}\odot}}{n_{\mathrm{e}}(r')}\right)^{1/4}\mathrm{d}r'. \tag{20}$$

At high frequencies, $x \ll I(x,\tau)^{1/2}\tau$, we have $I(x,\tau) \approx 1/\tau^{2/3}$ meaning that the approximation is valid if $x \ll \tau^{2/3}$, i.e., at $f \gg f_{\mathrm{c}}(r)$. The solution yields the power spectrum in form

$$P(f,r) = P_{\mathrm{WKB}}(f,r)\left(\frac{f_{\mathrm{c}}}{f}\right)^{2/3}, \quad f \gg f_{\mathrm{c}}(r). \tag{21}$$

The analytical theory can, thus, describe how the point of the spectral break from a $1/f$ to a $1/f^{5/3}$ spectral form behaves as a function of radial distance from the Sun. The generalization of the result to the case of initial power spectrum $\propto 1/f^q$ with other values of the spectral index q is discussed in Appendix A.

3.2. Approximate solution for the diffusive cascade

Following the result for the convective cascade, we assume that also in the case of a *diffusive* cascade the spectrum can be divided in two ranges: at low frequencies, $f < \tilde{f}_{\mathrm{c}}$ the cascade is inefficient and the wave power evolves according to WKB theory. At higher frequencies, the cascade has efficiently transformed the spectrum to its inertial form of $P \propto f^{-5/3}$. Therefore, we approximate the spectrum with a double power law,

$$P(f,r) \approx \begin{cases} P_{\mathrm{WKB}}(f,r), & f < \tilde{f}_{\mathrm{c}}(r) \\ P_{\mathrm{WKB}}(f,r)\left(\dfrac{\tilde{f}_{\mathrm{c}}}{f}\right)^{2/3}, & f \geq \tilde{f}_{\mathrm{c}}(r), \end{cases} \tag{22}$$

where we assume a single power law for the initial power spectrum given by Eq. (16). This spectral form allows us to estimate the break-point frequency, $\tilde{f}_{\mathrm{c}}(r)$, analytically, as follows.

Evaluate the terms of Eq. (5) for the solution (22) to get

$$\frac{v_{\mathrm{A}}}{AV}\frac{\partial}{\partial r}\left(\frac{AV^2}{v_{\mathrm{A}}}P\right) \approx H\left(f - \tilde{f}_{\mathrm{c}}\right)\frac{2V}{3\tilde{f}_{\mathrm{c}}}\frac{\mathrm{d}\tilde{f}_{\mathrm{c}}}{\mathrm{d}r}\left(\frac{\tilde{f}_{\mathrm{c}}}{f}\right)^{2/3}P_{\mathrm{WKB}}, \tag{23}$$

and

$$\frac{\partial F}{\partial f} \approx H\left(\tilde{f}_{\mathrm{c}} - f\right)\frac{2\pi\tilde{C}^2 v_{\mathrm{A}}}{V}\left(\frac{fP_{\mathrm{WKB}}}{B^2}\right)^{1/2} fP_{\mathrm{WKB}}, \tag{24}$$

where $H(f)$ is the Heavisde step function. While the approximation is *not* a solution of the wave transport equation, we can calculate the *position of the break point* in the power spectrum by assuming that the corresponding terms of the exact solution at $f = \tilde{f}_{\mathrm{c}}$ are well estimated (up to numerical constants of the order unity) by the values obtained from the approximation. This yields

$$\frac{1}{\tilde{f}_{\mathrm{c}}^2}\frac{\mathrm{d}\tilde{f}_{\mathrm{c}}}{\mathrm{d}r} \approx -a\frac{3\pi\tilde{C}^2 v_{\mathrm{A}}}{V^2}\left(\frac{\tilde{f}_{\mathrm{c}}P_{\mathrm{WKB}}(\tilde{f}_{\mathrm{c}},r)}{B^2}\right)^{1/2}, \tag{25}$$

where a is an adjustable constant of the order unity.

Making use Eqs. (16) and (19), we get

$$\frac{1}{\tilde{f}_{\mathrm{c}}^2}\frac{\mathrm{d}\tilde{f}_{\mathrm{c}}}{\mathrm{d}r} \approx -a\frac{3\pi\tilde{C}^2 V_\odot v_{\mathrm{A}}\epsilon_P^{1/2}}{V^3}\left(\frac{n_{\mathrm{e}\odot}}{n_{\mathrm{e}}}\right)^{1/4} \tag{26}$$

which can be integrated for $\tilde{f}_{\mathrm{c}}$ as

$$\frac{1}{\tilde{f}_{\mathrm{c}}} \approx 3\pi a\epsilon_P^{1/2}\int_{r_\odot}^{r}\frac{\tilde{C}^2(r')V_\odot v_{\mathrm{A}}(r')}{V^3(r')}\left(\frac{n_{\mathrm{e}\odot}}{n_{\mathrm{e}}(r')}\right)^{1/4}\mathrm{d}r'. \tag{27}$$

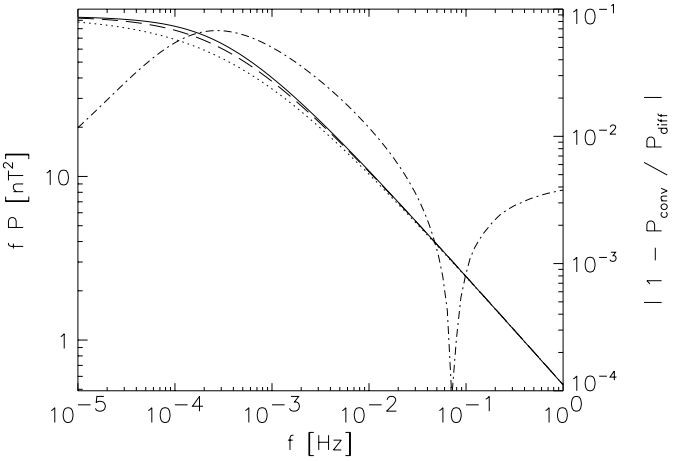

Fig. 2. Wave power spectrum at 0.3 AU from diffusive (solid curve) and convective (dashed curve) cascade models. The dash-dotted line represents the relative difference between the two. The dotted curve gives the approximate analytical form, Eq. (30).

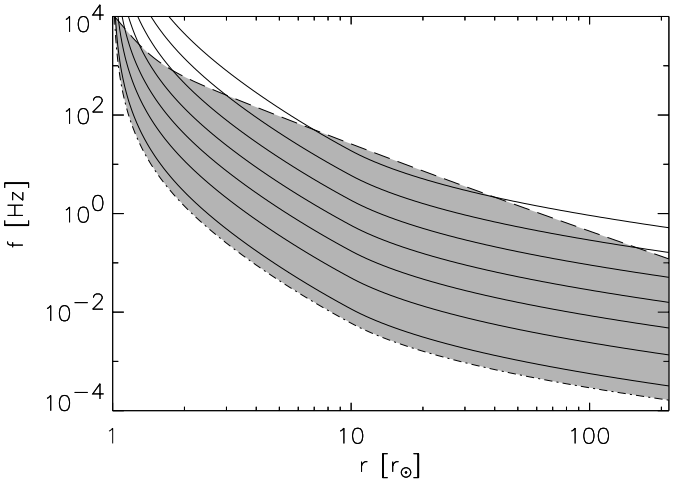

Fig. 3. Contours (at levels of $10^{-i/3}$ with $i = 1, 2, \ldots, 7$) of the normalized wave spectrum from diffusive cascade simulations, and the spectral break-point frequency (f_b of Eq. (28)) as obtained from the simulation (dashed curve). The inertial range, limited by the analytical approximation ($\tilde{f}_c$ of Eq. (27) with $a = 10/9$, i.e., f_c of Eq. (20)) for the break-point frequency and the dissipation frequency f_H (dashed curve), is shown by the gray area.

This is, thus, the equation for the break point in the diffusive cascade model. Taking into account that $\tilde{C}^2 = \frac{3}{5}C^2$, a value of $a = 10/9$ would yield an agreement between the models in the inertial range, i.e., $\tilde{f}_c(a = \frac{10}{9}) = f_c$.

The generalization of the result to other power-law forms of the initial power spectrum is again sketched in Appendix A.

4. Results

We have performed simulations of the transport of turbulence in the diffusive cascade model and compared our analytical formulation against them. We first analyze the convective and diffusive approaches by comparing our simulations to the exact convective flux solution, and then estimate the validity of the analytical approximation presented for the diffusive cascade. After that, we apply the method to solar wind wave heating and acceleration, as well as energetic particle transport. For a description of the numerical solution procedures, see Appendix B.

4.1. Comparison of model approaches

We first compare the spectral form of the diffusive approach to the analytical solution of the convective model of a turbulent cascade. For this, we have performed simulations using the following solar wind and cascade parameters. For the background solar wind, we choose the slow-wind example with $V = 400$ km s^{-1} discussed in Sect. 2.1 (Fig. 1) and the initial spectrum and wave transport parameters to match those by Hu et al. (1999). Thus, we choose the power spectrum parameter $\epsilon_P = 5 \times 10^{-5}$, the cascade parameters $\alpha_0 = 0.05$ and $\eta = 1$.

In Fig. 2, we show the spectra resulting from both cascade models at the distance of 0.3 AU. The agreement between the models, after the adjustment of the cascade constant discussed in Sect. 2.2, is remarkably good. As shown by the dash-dotted line in Fig. 2, the difference is less than 7% everywhere, and $\Delta = 0.005$ in the inertial range, the diffusive spectrum being below the convective one. We can obtain the break-point frequency, f_b, for the considered broken power-law spectrum, $P(f, r)$, as the frequency fulfilling $P(f_{in}, r) = P_{WKB}(f_{in}, r)(f_b/f_{in})^{2/3}$. Here f_{in} is a frequency deep in the inertial range, where the spectral index is 5/3. Thus,

$$f_b = f_{in}\left[\frac{P(f_{in}, r)}{P_{WKB}(f_{in}, r)}\right]^{3/2}. \quad (28)$$

By noting that $a = \frac{10}{9}(f_c/\tilde{f}_c)$, we can fix the value of a in Eq. (27):

$$a = \frac{10}{9}\left[\frac{P_{conv}(f_{in})}{P_{diff}(f_{in})}\right]^{3/2} = \frac{10}{9}(1+\Delta)^{3/2} \approx 1.12. \quad (29)$$

Since the diffusively simulated spectrum is only 0.5% different from the convective model in the inertial range, the break points in the convective and diffusive models differ by less than 1%. It can not be excluded that the difference is due to numerical inaccuracies of the diffusive simulations. Our study, thus, indicates that both models essentially capture the same physics.

We next compare the simulations with our analytical modeling of the break-point frequency (Eq. (27)) as a function of distance. In Fig. 3, we show the spectrum over the whole integration range as a contour plot. The WKB spectrum, Eq. (19), has been divided out in order to show only the evolution of the inertial range. Here we have taken $P = P_{diff}$ and $f_{in} = 10^5$ Hz in Eq. (28), and used $f_2 = 10^8$ Hz for the maximum frequency on the numerical grid. The figure shows that $\tilde{f}_c$ from Eq. (27) with $a = 10/9$ (i.e., f_c of Eq. (20)) traces the spectral break point of the simulations very well. (The above-derived errors of less than 1% are not visible on this scale.)

As compared to the spectra by Hu et al. (1999), our cascade is somewhat faster, resulting in about half an order of magnitude lower level of the inertial-range power spectrum. This, however, does not reflect any numerical problems (of ours or theirs), but is due to the slower wind in our model: besides

increasing the value of the flux function, decreasing the solar wind speed increases the time it takes for the wind to reach the observer, so the spectrum is more "aged" in our case than that of Hu et al. (1999). This effect is also observed in the solar wind, when comparing the power spectra in slow and fast solar wind streams at a fixed distance (e.g., Horbury 1999).

4.2. Applications

In the following applications, we evaluate three physical variables related to the Alfvénic turbulence: the heating functions due to ion-cyclotron resonances, the wave pressure, and the mean free path of the solar energetic particles. As shown in the previous section, the spectral break point of the diffusive model is well approximated by the exact result of the convective cascade recovered by choosing $a = 10/9$ in Eq. (27). We, thus, make use of the break-point frequency governed by Eq. (20), but model the spectrum with a smoothly behaving form,

$$P(f,r) = \frac{P_{\rm WKB}(f,r)}{1+[f/f_{\rm c}(r)]^{2/3}}, \tag{30}$$

where $P_{\rm WKB}(f,r)$ is given by Eqs. (16) and (19). For comparison with the exact spectral shapes, this form is also plotted in Fig. 2, and the agreement is seen to be satisfactory. Although the break-point frequency in the diffusive cascade model could also be calculated using this trial form of the power spectrum, we notice that this is unnecessarily complicated, since the additional numerical factors entering Eq. (27) can be absorbed in the constant a. All the analytical approximations below are calculated for both solar wind streams depicted in Fig. 1.

4.2.1. Heating functions

The analytical formulation of the cascade can readily be implemented for determining the heating rate of solar wind by dissipation at cyclotron resonance. Tu (1987) derived the heating rate due to dissipation and cascade at cyclotron resonance as

$$Q = Q_{\rm c} + Q_{\rm s} = \frac{F(f_{\rm H},r)}{4\pi} - V\frac{{\rm d}f_{\rm H}}{{\rm d}r}\frac{P(f_{\rm H},r)}{4\pi}, \tag{31}$$

where the second term represents the heating due to the decrease of the dissipation frequency, $f_{\rm H}$, with heliospheric distance and the first term the cascading of wave power into the dissipation region. Hereafter, we refer to the first one as the *cascade term* and to the second one as the *cyclotron sweep term* (Tu & Marsch 1997). A conventional way of choosing the dissipation frequency is to take it as a fixed fraction of the local ion cyclotron frequency. We, however, use a recent model (Vainio & Laitinen 2001; Laitinen et al. 2003), which incorporates the thermal dependence of cyclotron resonance by calculating the dissipation frequency from the quasilinear damping rate, $\gamma(f,r)$, of the Alfvén waves as $V/2\gamma(f_{\rm H},r) = r - r_\odot$, i.e., equating the damping length with the distance traveled by the wave. The proton temperature, $T_{\rm p}$, is modeled using a fit to the results of Tu & Marsch (1997) for a cyclotron heated solar wind stream with an asymptotic speed of 550 km s^{-1}, an intermediate value between the two models considered in this work. Thus, we use

$$v_{\rm p} = \frac{75.5\,R^{2.8} + 40.1\,R^{-5.4}}{\left(1 + 0.132\,R^{5.55} + 0.0222\,R^{6.3}\right)^{1/2}}\ {\rm km\ s^{-1}} \tag{32}$$

for the proton thermal velocity, $v_{\rm p} = \sqrt{2\,k_{\rm B}T_{\rm p}/m_{\rm p}}$, with $R = r/r_\odot$ and $k_{\rm B}$ being the Boltzmann constant. The calculated $f_{\rm H}$ is the upper boundary (dashed line) of the shaded inertial frequency range in Fig. 3.

The derivation of the cascade term requires simply the value of the flux function (Eq. (6) or (7)) at the dissipation frequency $f_{\rm H}$. The result is

$$Q_{\rm c} \approx \begin{cases} \dfrac{C^2}{2}\dfrac{v_{\rm A}}{V} f_{\rm H}^{5/2}\dfrac{P_{\rm H}^{3/2}}{B}, & \text{convective} \\ \dfrac{\tilde{C}^2}{2}\dfrac{v_{\rm A}}{V} f_{\rm H}^{5/2}\dfrac{P_{\rm H}^{3/2}}{B}\,\phi(f_{\rm c}/f_{\rm H}), & \text{diffusive,} \end{cases} \tag{33}$$

where $\phi(x) = 1 + \frac{2}{3}[1 + x^{2/3}]^{-1}$ and $P_{\rm H}(r) = P\big(f_{\rm H}(r), r\big)$ is computed from Eq. (30). The term can be simplified by using Eq. (20) if $f_{\rm c} \ll f_{\rm H}$. Then the cascade term for both models reduces to

$$Q_{\rm c} \approx -\frac{V}{f_{\rm c}}\frac{{\rm d}f_{\rm c}}{{\rm d}r}\frac{f_{\rm c}P_{\rm WKB}(f_{\rm c})}{4\pi}, \quad f_{\rm H} \gg f_{\rm c}. \tag{34}$$

Comparing this form to the cyclotron sweep term in the same limit, i.e.,

$$Q_{\rm s} \approx -\frac{V}{f_{\rm H}}\frac{{\rm d}f_{\rm H}}{{\rm d}r}\frac{f_{\rm H}P_{\rm WKB}(f_{\rm H})}{4\pi}\left(\frac{f_{\rm c}}{f_{\rm H}}\right)^{2/3}, \quad f_{\rm H} \gg f_{\rm c}, \tag{35}$$

shows the dominance of the cascade heating in our model: since $fP_{\rm WKB}(f,r)$ is independent of f and $(1/f_{\rm c})\,{\rm d}f_{\rm c}/{\rm d}r \sim (1/f_{\rm H})\,{\rm d}f_{\rm H}/{\rm d}r \sim 1/r$, the ratio of the sweep and cascade terms is of the order of $(f_{\rm c}/f_{\rm H})^{2/3}$, when the dissipation frequency lies far in the inertial range.

We present the heating functions in Fig. 4 for the diffusive model, and compare them to the heating function of the pure cyclotron sweep model, i.e., a model applying the sweeping mechanism to non-cascading (WKB) waves ($F = 0$), in the same two solar wind streams. As can be seen, for the specified cascade, the heating by the sweep process is always below the heating caused by the cascade. Note that in the case of the pure cyclotron sweep model in the slow wind, the heating is almost as efficient as the total heating in the case of cascading apart from the region near the coronal base. This can be understood by comparing the approximate form of the cascade term, Eq. (34), with that of the the sweep term, Eq. (35), and noting that in the case of no cascading, the fraction $(f_{\rm c}/f_{\rm H})^{2/3}$ should be omitted from the sweep term. The predicted wave power level in the dissipation range in the case of the pure cyclotron sweep model, however, contradicts observations in the solar wind, so at least at $r \gtrsim 0.3$ AU, this model is not an option. For the fast-wind model, cascading increases heating considerably at distances below $\sim$10 $r_\odot$ relative to the pure cyclotron sweep model. The total heating rate at these distances is about three times the corresponding heating rate in the slow-wind model.

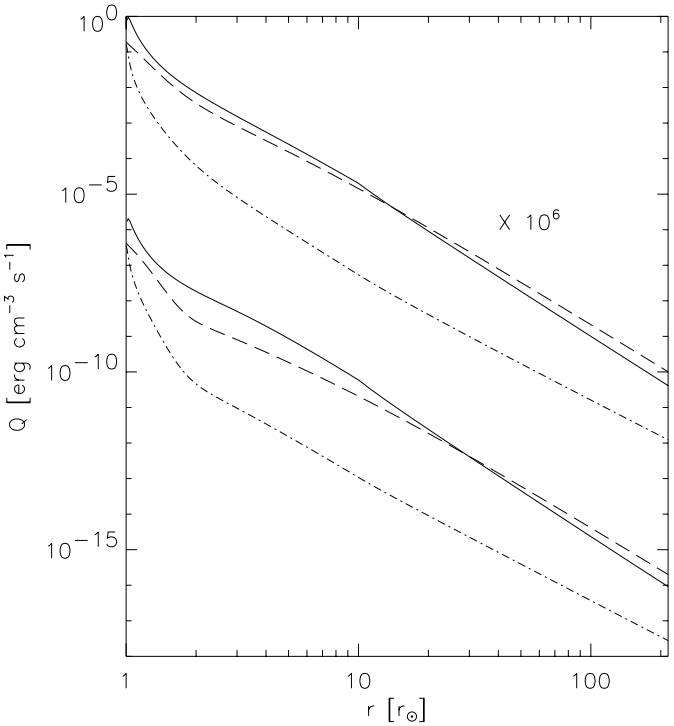

Fig. 4. Cascade (solid curves) and sweep (dash-dotted curves) components of the heating function, both plotted using the analytical approximation of the diffusive cascade. For comparison, we present the heating function in the case of no cascading applied (dashed curves). The results for the slow-wind model are multiplied by 10^6 as indicated in the figure.

Compared to the heating functions calculated using the exact spectra (slow-wind model), the analytical heating rates differ by less than 10% for both cascade models, so they provide an efficient alternative for numerical steady-state models of solar wind expansion.

4.2.2. Wave pressure gradient

In models of solar wind expansion driven by Alfvén waves, a considerable part of the momentum deposited to the solar wind comes from the gradient of the pressure of the Alfvén waves. This gradient consists of two parts. One is due to the decay of the wave pressure due to WKB-transport effects representing non-resonant interaction between the fluid and the wave. The other, resonant part is due to the loss of wave energy to the particles by heating.

Also the wave pressure can be estimated using our analytical formulation. The wave pressure is defined as

$$p_{\rm w}(r) = \frac{1}{8\pi}\int_0^\infty P(f,r)\,{\rm d}f = \frac{1}{8\pi}\int_{f_1}^{f_{\rm H}} P(f,r)\,{\rm d}f, \qquad (36)$$

where f_1 is the lower cutoff frequency of the spectrum, and the most straightforward way of calculating it in the case of a cascaded spectrum is to use numerical integration. The integral can also be analytically calculated in the case of our broken power law approximation, Eq. (30). This would, however, be a non-general formulation, since a spectrum with more complicated initial shape might not be easily integrated. Instead, we consider an alternative method, that is consistent with the computed heating functions, above.

To compute the wave pressure, we first note that it can be obtained also from an alternative formulation of the heating function (Hollweg 1973, 1986; Hollweg & Johnson 1988; Tu 1987):

$$Q = -\frac{v_{\rm A}}{VA}\frac{\rm d}{{\rm d}r}\left(\frac{AV}{v_{\rm A}}V\frac{\left\langle b^2\right\rangle}{4\pi}\right), \qquad (37)$$

where $\left\langle b^2\right\rangle = 8\pi\, p_{\rm w}$. Thus, by integrating the equation we find for the wave pressure:

$$p_{\rm w} = \frac{v_{\rm A}}{v_{\rm A\odot}}\frac{A_\odot}{A}\frac{V_\odot^2}{V^2}p_{\rm w\odot} - \frac{v_{\rm A}}{2V^2A}\int_{r_\odot}^{r}\frac{V'A'}{v'_{\rm A}}Q'\,{\rm d}r', \qquad (38)$$

where the primed quantities other than r' are values taken at $r = r'$, e.g., $A' = A(r')$. We present the specific acceleration, $-(m_{\rm p}n_{\rm e})^{-1}\partial p_{\rm w}/\partial r$, caused by the wave pressure, in Fig. 5 for the diffusive model using Eq. (38) for both the slow-wind stream and the fast-wind stream. When evaluating the wave pressure, $f_1 = 3\times10^{-5}$ Hz is used for the low-frequency cutoff at the Sun. For comparison, we have also plotted the same result for the pure cyclotron sweep model, the acceleration caused by the thermal proton pressure computed using the modeled temperature profile (Eq. (32) with $p_{\rm p} = \frac{1}{2}m_{\rm p}n_{\rm e}v_{\rm p}^2$), and the acceleration due to the gradient of the total pressure, $-(m_{\rm p}n_{\rm e})^{-1}(\partial p_{\rm tot}/\partial r) = u(\partial u/\partial r) + GM_\odot/r^2$, where G and $M_\odot$ are the gravitational constant and solar mass. It is seen that for our slow-wind model, the thermal pressure gradient dominates the acceleration. For the fast-wind model with a lower density, the situation is different: thermal pressure dominates only close to the coronal base, at $r < 2\ r_\odot$. Also the difference between the cascade models is larger in the case of the fast find than in the case of the slow wind. Although our models have different densities from the model of Tu & Marsch (1997), used here to describe the temperature, they produce rather reasonable values of the acceleration due to thermal pressure. For the fast wind the thermal pressure gradient is probably too small because of a low temperature. Note, however, that near the coronal base, at least, the gradient of electron pressure should also be considered, and it should bring up the sum of the thermal pressure gradients closer to the total pressure gradient consistent with the flow profiles.

The difference between the approximated wave pressure and the exact results is a few percent, which again proves the usefulness of analytical approaches to solar wind modeling.

4.2.3. Solar energetic particle transport

Vainio & Laitinen (2001) noted that there is a close connection between the cyclotron heating mechanism and the transport of solar energetic particles: the same high-frequency Alfvén waves required for the heating of the corona would efficiently scatter the energetic particles because of the cyclotron resonances. The calculated energetic-particle mean free paths for cyclotron heating models without cascading were shown to be orders of magnitude smaller than any values consistent with

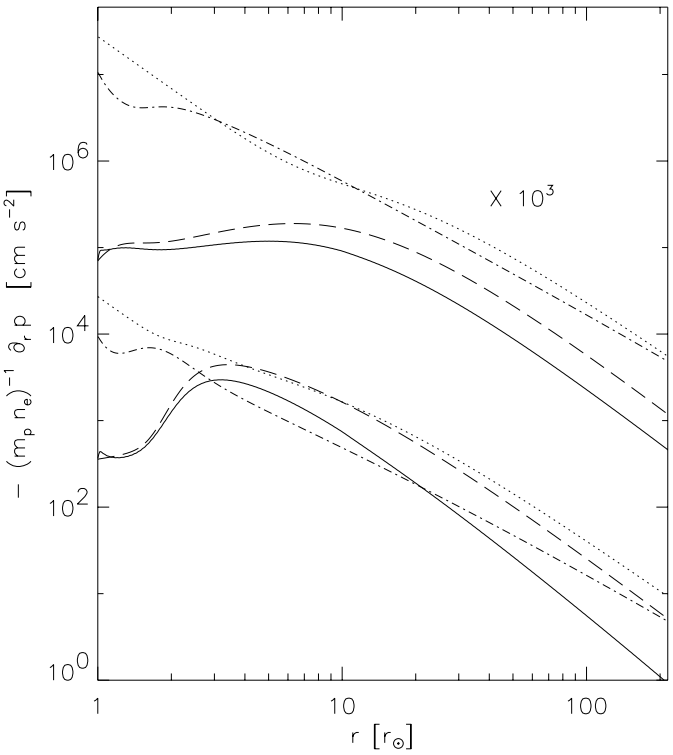

Fig. 5. The specific acceleration due to the wave pressure gradient computed using the analytical approximation of the diffusive cascade (solid curves). The same result for a pure cyclotron sweep model (dashed curves), and the acceleration due to the gradients of the thermal proton pressure (dash-dotted curves) and the total pressure (dotted curves) are plotted for comparison. The results for the slow-wind model are multiplied by 10^3 as indicated in the figure.

observations of solar energetic particle events. Since cascading can reduce the level of the power spectrum at resonant frequencies without resulting in a decrease of wind heating or acceleration, it was concluded by Vainio & Laitinen (2001) that spectral energy transfer could potentially resolve this discrepancy.

The energetic-particle mean free path, determining the strength of particle scattering by turbulence, is (e.g., Schlickeiser 2002)

$$\lambda = \frac{3v}{8}\int_{-1}^{+1}\frac{\left(1-\mu^2\right)^2}{D_{\mu\mu}}\,\mathrm{d}\mu, \tag{39}$$

where $D_{\mu\mu}$ is the particles' pitch-angle diffusion coefficient, v is the particle speed and μ the particle pitch-angle cosine. In the case of Alfvén waves propagating outward from the Sun, $D_{\mu\mu}$ can be given under quasi-linear approximation as (Vainio & Laitinen 2001)

$$D_{\mu\mu} = \frac{\pi}{4}\Omega\left(1-\mu^2\right)\frac{f_\mathrm{r}P(f_\mathrm{r},r)}{B^2}, \tag{40}$$

where Ω is the particles' (relativistic) gyrofrequency, and

$$f_\mathrm{r} = \frac{\Omega}{2\pi}\frac{V}{v|\mu|} \tag{41}$$

is the resonant wave frequency. Here, v and μ are measured in the frame co-moving with the Alfvén waves. We have also assumed that Alfvén waves have a zero net magnetic helicity, i.e.,

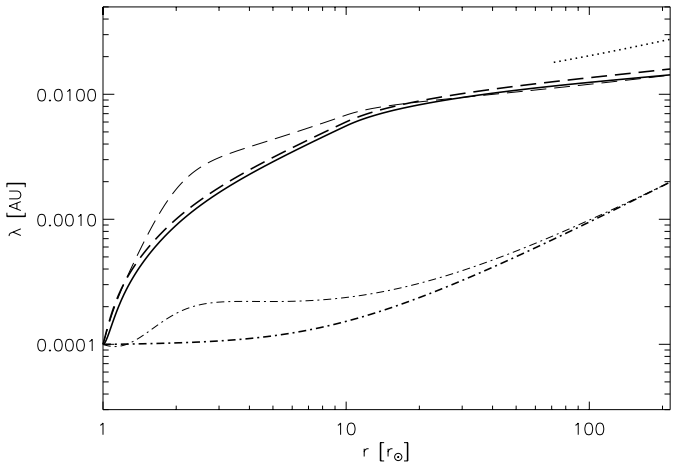

Fig. 6. Mean free path of 10 MeV protons computed using the exact diffusive-cascading solution (solid curve) and the approximation, Eq. (30), (dashed curves) for the power spectrum. The mean free path resulting from WKB-waves (dot-dashed curves) and from an observational trend of f_c (dotted curve) are given for comparison. The thick [thin] curves are computed for the slow [fast] wind model.

that both the left- and right-handed Alfvén waves have equal power spectra, $P^\mathrm{R}(f,r) = P^\mathrm{L}(f,r) \equiv \frac{1}{2}P(f,r)$. This assumption is equivalent of considering Alfvén waves with linear polarization, which they have already at very small propagation angles ($\theta > 2\sqrt{\omega/\Omega_\mathrm{p}}$) relative to the ambient magnetic field.

In the quasi-linear formulation, the pitch-angle diffusion coefficient is zero in a region near $\mu = 0$, which results in an infinite mean free path. Scattering off inward-propagating waves (Vainio 2000), or resonance broadening due to damping effects (Schlickeiser & Achatz 1993) or spectral energy transfer (Bieber et al. 1994) can, however, close the resonance gap near $\mu = 0$. We have modeled the scattering by extrapolating the power spectrum as $P(f) \propto f^{-5/3}$ as $f \to \infty$, thus filling the resonance gap caused by cyclotron damping. As some models predict substantially less scattering inside the resonance gap, our calculation represents a lower limit to the mean free path in the solar wind stream with the chosen parameters.

We computed the mean free path using both the diffusively simulated power spectrum and its analytical approximation, Eq. (30). The latter results in

$$\begin{aligned}\lambda &= \frac{2}{\pi}\frac{v}{\Omega}\left[1+\frac{27}{7}\left(\frac{\Omega V}{2\pi f_\mathrm{c} v}\right)^{2/3}\right]\frac{B^2}{(fP_\mathrm{WKB})(r)}\\ &= \frac{2}{\pi\epsilon_P}\frac{v}{\Omega}\left[1+\frac{27}{7}\left(\frac{\Omega V}{2\pi f_\mathrm{c} v}\right)^{2/3}\right]\left(\frac{n_\mathrm{e}}{n_{\mathrm{e}\odot}}\right)^{1/2}\frac{V^2}{V_\odot^2}.\end{aligned} \tag{42}$$

The value of the mean free path of 10 MeV protons for the simulated diffusive cascade spectrum is plotted in Fig. 6 along with this approximation. For comparison, we have plotted also the mean free path resulting from WKB wave transport, given by the first term in Eq. (42). Both solar wind models produce relatively similar mean free paths, the fast-wind values being above the slow-wind values near the position of the Alfvén speed maximum, as expected from Eq. (42). A mean free path of $\lambda \sim 0.015$ AU at $r = 1$ AU gives a diffusion time scale of $\tau_\mathrm{d} \sim r^2/2\lambda v \approx 30$ h for 10 MeV protons in the solar wind,

which is about an order of magnitude too long to account for observations of "standard" energetic particle events at 1 AU. This discrepancy between the model results and observations can be expected as is discussed in the following section.

5. Discussion and conclusions

We have calculated a semi-analytical expression for the power spectrum of cascading Alfvén waves in the coronal and solar wind plasma. The approximation is based on a description of the evolution of the break point of the power spectrum that is based on Tu et al.'s (1984) model of Alfvén-wave transport in the interplanetary medium. We restrict our study to flux functions reproducing the Kolmogorov spectrum supported by observations of power spectra in the interplanetary medium. The spectral break-point frequency f_c at the boundary of the energy-containing and inertial ranges of the spectrum evolves according to a simple integral, Eq. (20), that can be easily evaluated using standard numerical methods. As might be anticipated, the two forms of the Alfven-wave flux function, F, appearing in the literature and given by Eqs. (6), (7), and (8), do not result in significantly different power spectra, provided that the cascading constants are tuned to give the same flux in the inertial range, $f \gg f_c$.

We parametrize the spectrum with a convenient functional form, Eq. (30), to calculate the resulting heating functions, wave pressure and energetic-particle mean free path. We demonstrated that our semi-analytical treatment allows us to give these variables with a satisfactory accuracy without having to resort to numerical integration of the wave transport equation. For the heating function and the mean free path, we only have to solve the break-point frequency f_c, which can be done using standard numerical integration methods. For the wave pressure, one additional numerical integration (again using standard methods) of the computed heating function is required. The numerical evaluation of the heating and acceleration rates of the solar wind by this way is far more efficient than by solving partial differential equations of wave-energy, and we will use the methods developed here to generalize our steady-state solar wind model (Laitinen et al. 2003) to take into account wave cascading. The analytical description of the coronal and interplanetary mean free path of SEPs provides a model for the spatial and (high-)rigidity dependence of this parameter throughout the inner solar system.

We have chosen the parameters of the present cascade model so that the power spectrum exhibits a broken power law form with $P \propto f^{-1}$ below and $P \propto f^{-5/3}$ above a break-point frequency f_c, in agreement with observations of the solar wind MHD turbulence. According to observations made in the polar regions by Ulysses, this frequency scales like $f_c \propto r^{-1.1\pm0.1}$ (Horbury et al. 1996). For our slow-wind model with a constant α_1 in the solar wind, the break point scales as $r^{-0.70}$ near 1 AU and less steeply further out. This indicates that the assumption of constant α_1 might not be consistent with observations. We can translate the observed break point behavior as a function of distance to that of the cascade constant and, thus, α_1 by using Eq. (25). When using typical scaling laws for the solar wind parameters, $v_A \propto r^{-1}$, $n_e \propto r^{-2}$, and V constant, we get $\alpha_1 \propto r^{0.6\pm0.1}$. Thus, the normalized cross helicity, $\sigma_c = (1-\alpha_1^2)/(1+\alpha_1^2)$, should be decreasing with radial distance, consistent with observations in the solar wind (Bavassano et al. 1998). To give a quantitative example, we consider a break-point frequency scaling as $r^{-1.1}$ with a value of $f_c = 6.6 \times 10^{-5}$ Hz at 1 AU, obtained as an average of the measured values cited in Horbury et al. (1996). Using our slow-wind model, we compute the values of α_1 and σ_c between 0.1 and 1 AU (see Fig. 7). We note that while the cross helicity is a decreasing function of distance, the waves are still predominantly outward propagating inside 1 AU, and the small decrease of the cross helicity might not explain the observations. On the other hand, the smallness of α_1^2 is necessary for the applied connection to σ_c to be valid (Verma et al. 1995). It is also a necessary constraint for the present cascade models to be reasonable, as they do not treat the inward waves consistently.

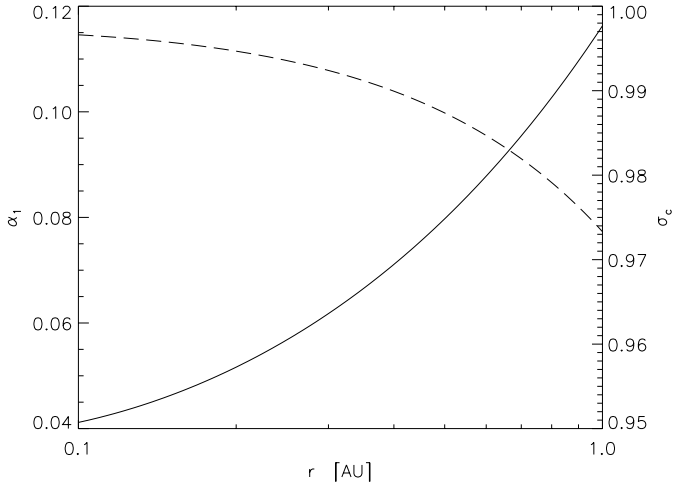

Fig. 7. Parameter α_1 (solid curve) and the resulting cross-helicity σ_c (dashed curve) computed for a break-point frequency f_c deduced from observations in the solar wind.

The results shown in Fig. 4 are very similar to those obtained by Hollweg & Johnson (1988) who, like us, considered heating of the solar corona and solar wind by cascading outward-propagating Alfvén waves. Similar results were also obtained by Dmitruk et al. (2002). They considered heating due to cascading in perpendicular wave number and found that the heating function is, via the Alfvén speed, related to the large-scale magnetic field and the solar wind density profile – like in the case of a parallel cascade studied in the present paper. So, as these authors concluded as well, while the heating function can be understood on the basis of turbulent cascading, a discrimination between the different heating models can as yet not be made. Note, however, that the inward/outward wave ratio, which in the present work is merely a model parameter, was self-consistently determined in the model of Dmitruk et al. (2002).

Although cascading is seen to provide a strong enhancement of the mean free path, it is still not enough (for the studied parameters) to produce values in agreement with typical SEP observations, i.e., $\lambda(1\text{ AU}) \gtrsim 0.1$ AU. This is, however, what one often observes in the solar wind: the mean free path calculated from a typical magnetic-field power spectrum

(assuming, as above, standard quasi-linear theory (QLT) with slab-mode fluctuations, i.e., $\boldsymbol{k} \parallel \boldsymbol{B}_0 \perp \delta\boldsymbol{B}$) is, on average, about an order of magnitude smaller than values typically obtained from SEP observations (e.g., Bieber et al. 1994). This may reflect the details of scattering across $\mu = 0$ (Schlickeiser & Achatz 1993; Vainio 2000), but it may also be due to the invalidity of the slab-mode waves as a description of the solar wind fluctuations (Bieber et al. 1994). However, a case-by-case comparison between the observed energetic-particle mean free path and the one computed (using slab-mode QLT) from the *simultaneously observed* magnetic-field power spectrum by Wanner & Wibberenz (1993) shows that in four of the studied eight energetic particle events, the two mean free paths agree within the accuracy of observations. These authors concluded that the slab-mode QLT can be considered a viable theory of SEP propagation. In reflection to our modeling, we note that increasing the value of the cascade constant and/or lowering the level of solar wave power can increase the modeled mean free paths to the typically observed levels. A model with a cascade constant increasing in the solar wind, consistent with the observed break-point scaling law $f_c \propto r^{-1.1}$ (see above), already yields larger values of the mean free path than obtained for our constant value (dotted curve in Fig. 6). To conclude whether our model is capable of explaining the global transport conditions, however, requires self-consistent modeling of the solar wind expansion and turbulence transport, which is left for the future.

Appendix A: The spectral break point for $P \propto f^{-q}$

Let us consider the spectral break point in the case of an initial spectrum of a power-law form,

$$P(f, r_\odot) = \frac{\epsilon_P B_\odot^2}{f_n} \left(\frac{f_n}{f}\right)^q \tag{A.1}$$

with $q < 5/3$. In the convective model, the dimensionless power spectrum at the Sun becomes

$$g(x) = (f/f_n)^{5/3-q} = x^{(3q-5)/2} \tag{A.2}$$

and the equation for I becomes

$$I(x,\tau) = \left[x + I^{1/2}(x,\tau)\tau\right]^{(3q-5)/2}. \tag{A.3}$$

If $x \gg I^{1/2}(x,\tau)\tau$, the solution is again $I = g(x)$, and WKB-propagation is recovered. In the other limit, $x \ll I^{1/2}(x,\tau)\tau$, the solution is $I(x,\tau) = \tau^{2(3q-5)/[3(3-q)]}$, i.e., $P(f,r) = P_{\rm WKB}(f,r)(f_g/f)^{5/3-q}$ for $f \gg f_g$, with

$$f_g(r) = f_n \tau(r)^{2/(q-3)}, \tag{A.4}$$

where $\tau(r)$ should be substituted from Eq. (13).

In the case of a diffusive cascade, the analysis starts from the assumption

$$P(f,r) \approx \begin{cases} P_{\rm WKB}(f,r), & f < \tilde{f}_g(r) \\ P_{\rm WKB}(f,r)\left(\dfrac{\tilde{f}_g}{f}\right)^{5/3-q}, & f \geq \tilde{f}_g(r). \end{cases} \tag{A.5}$$

Thus,

$$\frac{v_A}{AV}\frac{\partial}{\partial r}\left(\frac{AV^2}{v_A}P\right) \approx H\left(f-\tilde{f}_g\right)\frac{(5-3q)V}{3\tilde{f}_g}\frac{\mathrm{d}\tilde{f}_g}{\mathrm{d}r}\left(\frac{\tilde{f}_g}{f}\right)^{5/3-q} P_{\rm WKB}, \tag{A.6}$$

and

$$\frac{\partial F}{\partial f} \approx H\left(\tilde{f}_g - f\right)\frac{(5-3q)q}{2}\frac{2\pi\tilde{C}^2 v_A}{V}\left(\frac{fP_{\rm WKB}}{B^2}\right)^{1/2} fP_{\rm WKB}. \tag{A.7}$$

Taking these to be equal at $f = f_g$ gives

$$\frac{\mathrm{d}}{\mathrm{d}r}\left(\frac{\tilde{f}_g}{f_n}\right)^{(q-3)/2} = \frac{(3-q)q}{2}\frac{3\pi f_n \tilde{C}^2 v_A}{V^2}\left(\frac{f_n P_{\rm WKB}(f_n,r)}{B^2}\right)^{1/2} \tag{A.8}$$

leading, apart from numerical factors, again to the same form as the convective model, Eq. (A.4), for $q > 0$. Note, however, that the case $q \leq 0$ can not be handled by this way. In this case, the initial assumption on the form of the power spectrum is not a good one, since inverse cascading acts to spread the wave power also toward lower frequencies.

Appendix B: Solution procedures for wave transport equation

We numerically solve the diffusive wave transport equation using finite differencing on a grid with logarithmic spacing in both r and f. For the case of the diffusive cascade, Eq. (5) can be written in a dimensionless form as

$$\frac{\partial \tilde{I}}{\partial \tilde{\tau}} = \mathrm{e}^{-y}\frac{\partial}{\partial y}\mathrm{e}^{5y/2}\frac{\partial \tilde{I}^{3/2}}{\partial y}, \tag{B.1}$$

where

$$\tilde{I}(y,\tilde{\tau}) = P(f,r)\frac{\tilde{f}_n\, n_e^{1/2}(r)\, V^2(r)}{B^2(r)\, n_{e\odot}^{1/2}\, V_\odot^2} \tag{B.2}$$

$$y = \ln\left(f/\tilde{f}_n\right) \tag{B.3}$$

$$\tilde{\tau} = \frac{4\pi\tilde{f}_n}{3}\int_{r_\odot}^{r}\frac{\tilde{C}^2(r')V_\odot v_A(r')}{V^3(r')}\left(\frac{n_{e\odot}}{n_e(r')}\right)^{1/4}\mathrm{d}r' \tag{B.4}$$

and $\tilde{f}_n$ is an arbitrary normalization frequency. Note that $\tilde{\tau}(r) = \frac{2}{3}\epsilon_P^{-1}\tau(r) = \frac{2}{3}\epsilon_P^{-1} f_n/f_c(r)$, if we choose the present scaling frequency to match the one from the dimensionless convective approach, $\tilde{f}_n = f_n$. The grid values for y are evenly spaced and the grid values for $\tilde{\tau}$ can be computed from those of r using standard numerical integration methods. We choose $\tilde{f}_n$ to be the smallest frequency in the grid and, thus, take $y_k = k\Delta y$ with $k = 0, 1, 2, \ldots, N_k - 1$. The y-discretization becomes

$$\mathrm{e}^{-y}\frac{\partial}{\partial y}\mathrm{e}^{5y/2}\frac{\partial \tilde{I}^{3/2}}{\partial y} \approx \frac{\mathrm{e}^{3k\Delta y/2}}{(\Delta y)^2}\left\{\mathrm{e}^{5\Delta y/4}\left[\left(\tilde{I}_{k+1}\right)^{3/2} - \left(\tilde{I}_k\right)^{3/2}\right] - \mathrm{e}^{-5\Delta y/4}\left[\left(\tilde{I}_k\right)^{3/2} - \left(\tilde{I}_{k-1}\right)^{3/2}\right]\right\}. \tag{B.5}$$

The $\tilde{\tau}$-discretization is then done using an implicit scheme (adapted from Press et al. 1992) involving a tridiagonal matrix inversion to advance the solution from one $\tilde{\tau}$-level to the next. As boundary conditions, we take $\tilde{I} = 0$ outside the y-grid.

In order to solve the convective model, one has to obtain the solutions of $I(x,\tau)$ from Eq. (14), which requires the use of a non-linear root solver. In this paper, we have restricted the initial power spectrum to the form $\propto 1/f$ resulting in Eq. (18). This equation can, of course, be solved analytically in closed form, but for later generalization we have used a standard root solver. For positive x and τ, there is only one positive real root $I^{1/2}$ of the equation. We have solved the root at $x_k = (f_\mathrm{n}/f_k)^{2/3}$ and $\tau_i = f_\mathrm{n}/f_\mathrm{c}(r_i)$, where $\{(f_k, r_i)\}$ is the set of grid points used in the diffusive simulation, $f_\mathrm{n} = 10^{-6}$ Hz. The integral in Eq. (20) is performed using standard numerical methods.

Acknowledgements. The Academy of Finland (AF) is thanked for financial support of the projects 46331 and 51466. This study is a part of the project "Collective Processes in Astrophysical Plasmas: Waves, Heating and Accelerated Particles" co-funded by AF and Deutscher Akademischer Austauschdienst (DAAD). The authors wish to thank the referee for valuable comments and suggestions on the manuscript.

References

Bavassano, B., Pietropaolo, E., & Bruno, R. 1998, J. Geophys. Res., 103, 6521
Bieber, J. W., Matthaeus, W. H., Smith, C. W., et al. 1994, ApJ, 420, 294
Bird, M. K., & Edenhofer, P. 1990, in Physics of the Inner Heliosphere, vol. I, ed. R. Schwenn, & E. Marsch (Berlin Heidelberg: Springer-Verlag), 13
Chapman, S. 1957, Smithsonian Contrib. Astrophys., 2, 1
Dmitruk, P., Matthaeus, W. H., Milano, L. J., et al. 2002, ApJ, 575, 571
Hartle, R. E., & Barnes, A. 1970, J. Geophys. Res., 75, 6915
Hollweg, J. V. 1973, ApJ, 181, 547
Hollweg, J. V. 1986, J. Geophys. Res., 91, 4111
Hollweg, J. V., & Turner, J. M. 1978, J. Geophys. Res., 83, 97
Hollweg, J. V., & Johnson, W. 1988, J. Geophys. Res., 93, 9547
Hollweg, J. V., & Isenberg, P. A. 2002, J. Geophys. Res., 107 (A7), 10.1029/2001JA000270
Horbury, T. S. 1999, in Plasma Turbulence and Energetic Particles in Astrophysics. Obserwatorium Astronomiczne, ed. M. Ostrowski, & R. Schlickeiser (Kraków: Uniwersytet Jagielloński), 115
Horbury, T. S., Balogh, A., Forsyth, R. J., & Smith, E. J. 1996, A&A, 316, 333
Hu, Y. Q., Habbal, S. R., & Li, X. 1999, J. Geophys. Res., 104, 24819
Isenberg, P. A. 2001, J. Geophys. Res., 106, 29249
Laitinen, T., Fichtner, H., & Vainio, R. 2003, J. Geophys. Res., 108 (A2), 1081, DOI: 10.1029/2002JA009479
Leith, C. E. 1967, Phys. Fluids, 10, 1409
Liewer, P. C., Velli, M., & Goldstein, B. E. 2001, J. Geophys. Res., 106, 29261
Miller, J. A., & Roberts, D. A. 1995, ApJ, 452, 912
Press, W. H., Teukolsky, S. A., Vetterling, W. T., & Flannery, B. P. 1992, Numerical Recipes in Fortran 77: The Art of Scientific Computing, 2nd ed. (Cambridge University Press)
Schlickeiser, R. 2002, Cosmic Ray Astrophysics (Berlin Heidelberg: Springer-Verlag), 310
Schlickeiser, R., & Achatz, U. 1993, J. Plasma Phys., 49, 63
Schwenn, R. 1990, in ed. R. Schwenn, & E. Marsch, Physics of the Inner Heliosphere, vol. I (Berlin Heidelberg: Springer-Verlag), 99
Scudder, J. D. 1992, ApJ, 398, 299
Sittler, E. C., Jr., & Guhathakurta, M. 1999, ApJ, 523, 812
Tu, C.-Y. 1987, Sol. Phys., 109, 149
Tu, C.-Y. 1988, J. Geophys. Res., 93, 7
Tu, C.-Y., Pu, Z.-Y., & Wei, F.-S. 1984, J. Geophys. Res., 89, 9695
Tu, C.-Y., Roberts, D. A., & Goldstein, M. L. 1989, J. Geophys. Res., 94, 13575
Tu, C.-Y., & Marsch, E. 1997, Sol. Phys., 171, 363
Vainio, R. 2000, ApJS, 131, 519
Vainio, R., Kocharov, L., & Laitinen, T. 2000, ApJ, 528, 1015
Vainio, R., & Laitinen, T. 2001, A&A, 371, 738, 2001
van de Hulst, H. C. 1953, in The Sun, ed. G. P. Kuiper (Chicago: University of Chicago Press)
Verma, M. K., Roberts, D. A., & Goldstein, M. L. 1995, J. Geophys. Res., 100, 19839
Vocks, C., & Marsch, E. 2001, Geophys. Res. Lett., 28, 1917
Wanner, W., & Wibberenz, G. 1993, J. Geophys. Res., 98, 3513
Zhou, Y., & Matthaeus, W. H., J. Geophys. Res., 95, 14881